Understanding Polydirectional Aeolian Cross-Strata Architecture in a Coastal Unidirectional Wind Regime

8 authors, including:

Alexandre Medeiros de Carvalho
Universidade Federal do Ceará
36 PUBLICATIONS   **139** CITATIONS

SEE PROFILE

Vanda Claudino-Sales
Universidade Federal de Ceara
190 PUBLICATIONS   **962** CITATIONS

SEE PROFILE

Francisco Gleidson da Costa Gastão
Universidade Federal do Ceará
27 PUBLICATIONS   **30** CITATIONS

SEE PROFILE

Letícia Mesquita
Universidade Federal do Ceará
13 PUBLICATIONS   **1** CITATION

SEE PROFILE

Some of the authors of this publication are also working on these related projects:

Project   Is Brazilian wind power development sustainable? Insights from a review of conflicts in Ceará state View project

Project   Temporal morphodynamic and internal structure characterization of a barchan/barchanoid dunes using aerophotogrammetry, GPR and trenches in Flecheiras, Trairi – CE.
View project

Understanding Polydirectional Aeolian Cross-Strata Architecture in a Coastal Unidirectional Wind Regime

Alexandre Medeiros de Carvalho[†], Sérgio Bezerra Lima Júnior[†], Luis Parente Maia[†], Vanda Claudino-Sales[‡*], Francisco Gleidson da Costa Gastão[†], Letícia Mesquita Eduardo[†], Lidriana Pinheiro de Souza[†], and Marcus Vinicius Chagas da Silva[†]

www.cerf-jcr.org

[†]Institute of Marine Sciences, LABOMAR
Federal University of Ceará, UFC
Brazil

[‡]Geography Department
Federal University of Ceará, UFC
Brazil

ABSTRACT

Carvalho, A.M.; Lima Jr., S.B.; Maia, L.P.; Claudino-Sales, V.; Gastão, F.G.C.; Eduardo, L.M.; Souza, L.P., and Silva, M.V.C., 0000. Understanding polydirectional aeolian cross-strata architecture in a coastal unidirectional wind regime. *Journal of Coastal Research,* 00(0), 000–000. Coconut Creek (Florida), ISSN 0749-0208.

Crescentic dune fields along the NE coast of Brazil were analyzed to justify processes associated with the wide range of cross-strata dip directions in aeolian deposits found in a unidirectional wind regime. Multiple spatial and temporal field-based methodologies were employed, including trenching, ground penetrating radar (GPR), and photogrammetry. Wind dynamics, coastline morphology, bounding surface developing processes, and dune migration patterns were also considered. Analysis revealed a relationship between small- and large-scale morphologies of the crescentic dune field. The interactions of crescentic dune crests, in association with the superposition of multiple superposed dunes, explain the majority of cross strata and dip directions found in dune trenches and GPR sections. This study provides convincing evidence that microscale structures observed within trenches and GPR sections are compatible with the macroscale slipface position observed within the dune field. Small-scale changes in wind direction, caused by the dune crest morphologies themselves, explain much of the supposedly unexpected strata dip directions that arc through from 90° to 180°. The presence of near-surface water tables supports the formation and preservation of aeolian cross-strata sequences.

ADDITIONAL INDEX WORDS: *Crescentic dunes, cross strata, trenches, 3D GPR, dip directions, NE Brazil.*

INTRODUCTION

Multiple studies investigating small-scale aeolian transport rates, based on deterministic models and/or associated with dune dynamics, have been conducted in NE Brazil (*e.g.*, Barrineau and Ellis, 2013; Carvalho, 2003; Carvalho *et al.*, 2015; Durán and Herrmann, 2006; Jimenez *et al.*, 1999; Kok *et al.*, 2012; Kroy, Sauermann, and Herrmann, 2002; Levin *et al.*, 2009; Li, Ellis, and Sherman, 2014; Maia, 1998; Martin *et al.*, 2018; Pelletier *et al.*, 2015; Sauermann *et al.*, 2003; Schwämmle and Herrmann, 2004; Sherman *et al.*, 2013, 2018; Tsoar *et al.*, 2009). In spite of the importance of all these works for advancing the understanding of wind-blown sand dynamics, they do not focus on local variations in wind direction and the resulting wide range of cross strata and dip directions in a unidirectional wind regime. The lack of identification of these processes was seen in the substantial variability of aeolian strata dip directions found in local aeolianites (*e.g.*, Carvalho *et al.*, 2008) and the controversial "paleo-wind directions" aeolianites by Castro *et al.* (2017), in a region dominated by a unidirectional wind regime (Tsoar *et al.*, 2009).

Since Sorby (1859) related migrating bedforms to internal structures and external flow conditions and inferred sediment transport directions from orientations of internal structures,

the study of cross strata has revealed new developments. Important contributions were introduced by Allen (1962) with the development of models for interpreting cross-strata dip direction patterns for shallow marine and deltaic sediments. The study of cross strata can also provide information about the behavior of aeolian bedforms and how they interact with one another. The study is also important for fluid dynamics and modeling, since, as stressed by Rubin (1987), to produce accurate bedform flow interaction models, it is necessary to fully comprehend bedforms and flow behaviors. Narteau *et al.* (2009) used cellular automaton (CA) dune models focusing on the imprecision of the continuous dune models (*e.g.*, Durán, Schwammle, and Hermann, 2005; Hersen *et al.*, 2004) to reproduce dune interaction amalgamation and modelling of secondary bedforms induced by collisions.

To unveil the processes responsible for developing complex structures in the referred system, starting from the premise that the nature, extent, and spacing of ancient bounding surfaces and their hierarchical arrangement are incompatible with simple dune systems was considered (Brookfield, 1977). This is likely related to the migration of superposed protodunes and dunes on larger dunes, as well as interacting dune fields, as in the case of the studied area.

Brothers *et al.* (2017) recognized the interactions of dune crestlines, accompanied by the ejection of dune segments, as drivers in changing dune morphology. They considered that defect and bedform repulsion interactions have been misidentified or overlooked in the aeolian stratigraphic record. Brothers *et al.* (2017) also highlighted the need to expand

Fryberger, Schenk, and Krystinik, 1988; McKee, 1966; Stokes, 1968), and are also important for the origin and preservation of aeolian cross strata. Thus, the influence of the water table on dune succession (Mountney, 2012) as an element of wind deflation control, and therefore a consequent factor of depositional sequences or cross strata preservation, was observed and evaluated in this study.

This type of study requires investigation of the internal structures of aeolian deposits, whether directly through trenches, indirectly through ground penetrating radar (GPR) sections, or both. The first approach has proved to be effective and relatively inexpensive (*e.g.*, Bigarella, 1971, 1975; Bigarella, Becker, and Duarte, 1969; Kocurek *et al.*, 2007; McKee, 1966, 1979). The association of GPR and trenching in aeolian environments has been used worldwide (*e.g.*, Bristow, Pugh, and Goodall, 1996; Bristow, Chroston, and Bailey, 2000; Bristow and Pucillo, 2006; Clemmensen *et al.*, 2007; Girardi, 2005; Horwitz and Wang, 2005).

Thus, the purpose of this paper is to employ multiple spatial and temporal field-based methodologies to explain the variable dune crest migration directions and their resulting wide range of cross strata dip directions in a unidirectional wind regime along the NE coast of Brazil (Figure 1).

Study Area

The shoreline of the state of Ceará, NE Brazil, comprises sequences of headlands separating bays ranging in size from 10 to 30 km (Carvalho *et al.*, 2015) and that can be broadly classified as crenulate shaped (Hsu, Silvester, and Xia, 1989; Silvester, 1960, 1970; Silvester and Ho, 1972) or headland bay beaches (Yasso, 1965). The beaches (ranging from 50 to 300 m wide) are dissipative to intermediate, using the Wright and Short (1983) beach classification system. Beach deposits are predominantly fine and medium sand in equal proportions, with rare occurrences of coarse sand (Carvalho, 2003), and are at times bordered by foredunes. The local climatic regime, and therefore aeolian dynamics, is mainly related to the Inter-Tropical Convergence Zone (ITCZ) migration and meteorological conditions in the Northern Hemisphere, despite the study site's location in the Southern Hemisphere (CLIVAR/Brasil, 1998). From December to April, the region experiences its rainy season, when NE trade winds are significant, but not effective for sand transport. From July to November, the rain steadily diminishes until drought conditions are set and trade winds are predominately from E and ENE (Figure 1), becoming effective for sand transport.

These climatic and sedimentological conditions, coupled with large quantities of fine and medium sands, are favorable to the development of extensive dune fields. Tsoar *et al.* (2009) estimated that 78% of the annual winds in this region are above the threshold velocity for sand transport. They also calculated wind drift potential (DP) for wind directions above the threshold velocity and assigned a corresponding vector unit (v.u.), which is an estimate of the sand drift amount in a given direction. The total vector unit for all wind categories comprises the DP. During the wet season, DP is low (14% of the yearly DP); and during the dry season, DP is high (86% of the yearly DP). Tsoar *et al.* (2009) also noted that annual winds are easterly to southeasterly and produce an average drift
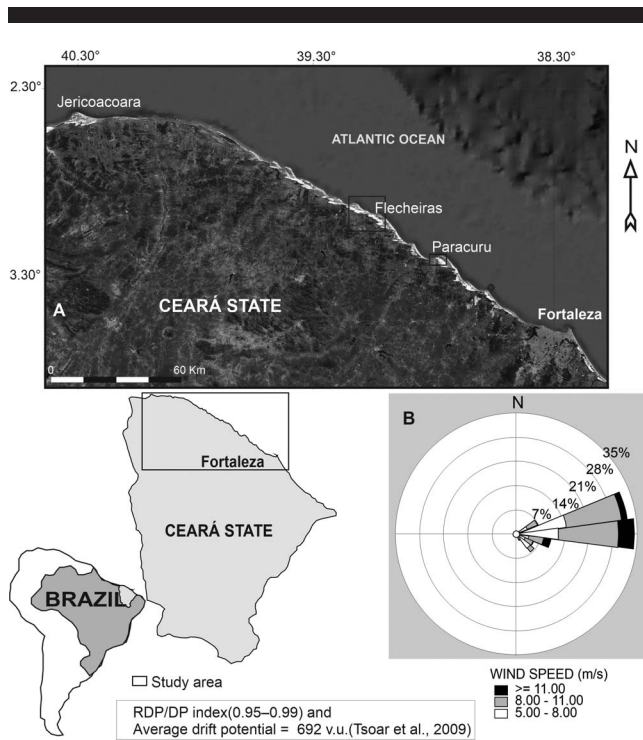

Figure 1. Coastal region of Ceará (in NE Brazil). The target area of this research is highlighted on the map. The wind rose only considers wind speeds above 5 m/s.

studies in this line of research to strengthen the model of dune stratigraphy to form a basis for the identification of dune interaction in the rock record. In this sense, Day and Kocurek (2017) presented a series of ancient rock records interpreted as aeolian dune interactions in Jurassic aeolian unities in the Western United States.

It is well known that large bedforms can modify fluid flow (Bagnold, 1941; Cooke and Warren,1973). Furthermore, there is the recognition that the interactions of barchan dunes, for instance, influence dune morphology (*e.g.*, Durán *et al.*, 2009; Elbelrhiti, Claudin, and Andreotti, 2005, 2008; Parteli *et al.*, in review). Hence, this is an important tool for expecting modifications on small protodunes, as well as dunes leeward of a larger dune.

Additional studies have extensively investigated complex dune interactions (*e.g.*, Brothers *et al.*, 2017; Ewing and Kocurek, 2010; Ewing, McDonald, and Hayes, 2015; Fenton *et al.*, 2014; Kocurek, Ewing, and Mohrig, 2010; Liu and Zimbelman, 2015; Zimbelman and Johnson, 2017), recognizing that dune topography does influence wind speed and direction (*e.g.*, Bauer *et al.*, 2013; Hesp *et al.*, 2005, 2015; Jackson, Bourke, and Smyth, 2015). Further investigations are required, particularly based on interactions among aeolian bedforms in the scale of protodunes and dunes, and the resulting cross strata in a unidirectional wind transport regime.

The development processes of bounding surfaces are often attributed to changes in wind characteristics, dune deflation, and migration, along with changes in groundwater level (*e.g.,*
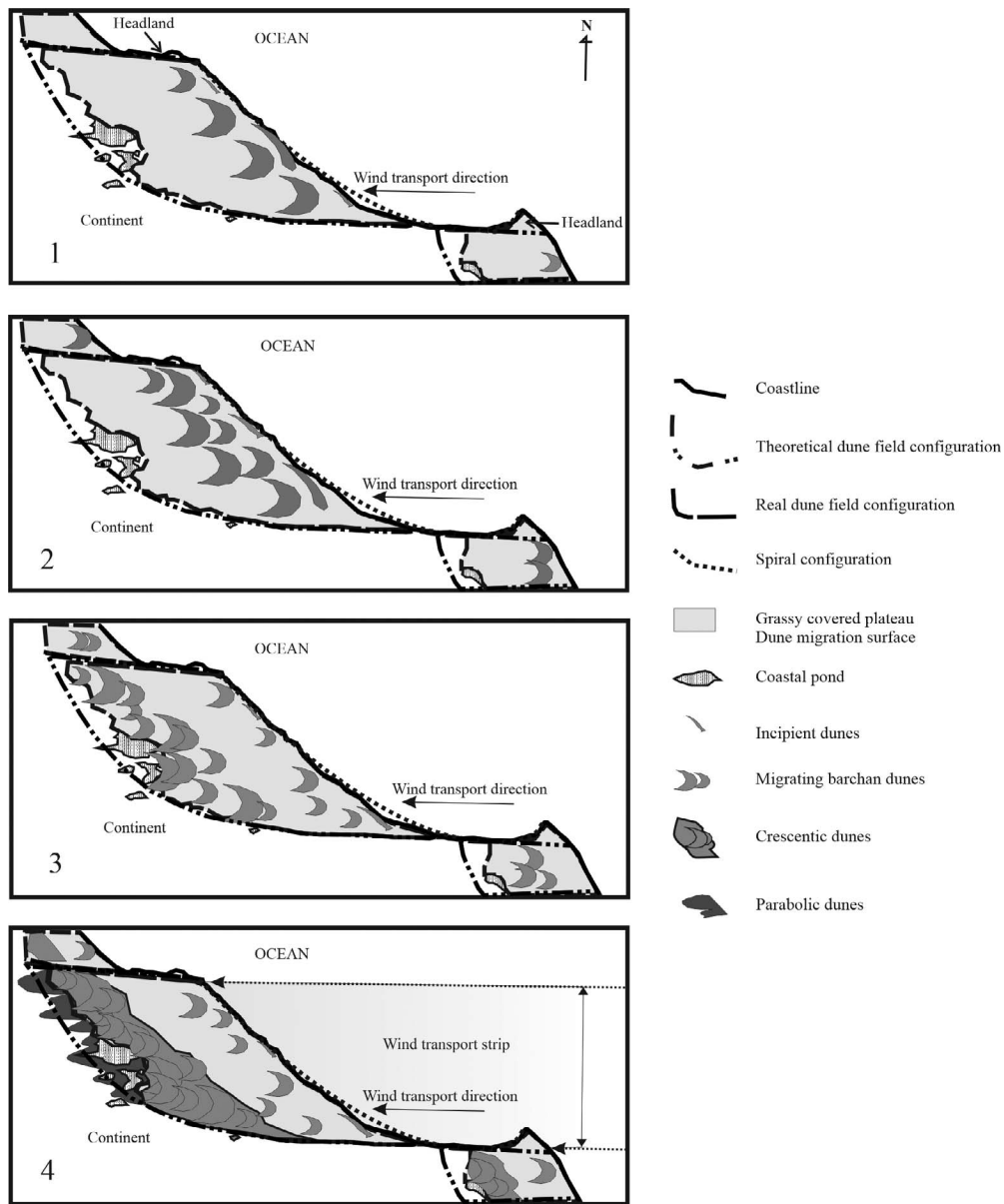
Figure 2. Dune migration patterns and evolutionary stages along the NW Ceará coast. Through time, the coast progresses from panel 1 to panel 4. Modified from Carvalho *et al.* (2015).

potential of 692 v.u. They estimated a "very high" (0.95–0.99) index of wind direction variability (resultant drift potential/drift potential [RDP/DP]) along the Ceará coast (Figure 1). This high index value, indicative of a unidirectional wind regime, is also ideal for parabolic and barchan dune development (*e.g.*, Bishop *et al*., 2002), which generates barchanoid dunes in which the maximum range of dip direction is less than 60°.

The unidirectional wind regime, associated with the crescent-shaped bays, has created wind transport sectors along the coast. Carvalho *et al*. (2015), following Bauer and Davidson-Arnott (2002), divided these coastal sectors into two segments associated with aeolian transport.

Dune Type and Evolution

A striking feature of wind activity in this region is the distribution of aeolian deposits within different bedforms and evolutionary sequences from the beach toward the continent's interior (Figure 2). These morphologies originate near the upper foreshore as small patchy embryo (or incipient) dunes without a well-defined shape. As they develop into foredunes and grow and migrate inland, their migration rate decreases and their sediment trapping rate increases. Barchans and barchanoid dunes form and continue to migrate over a partially grassy covered subhorizontal flat surface to a gently undulating plateau (Carvalho *et al*., 2015). Grassy covered plateaus

Figure 3. Large dune surface in Flecheiras, Ceará, Brazil. Barchan and barchanoid dunes of tens of meters wide migrate and overlap the larger dune's surface that measures more than 600 m wide and 400 m long. The prevailing wind direction is from left to right of the image.

(Figure 2) usually separate near-beach dunes from crescentic interacting barchan/barchanoid dune crests, developed in the penultimate dune forming stage. These mostly crescentic dunes form when large barchans and barchanoid dunes traverse the grassy plateaus, coalesce and interact, while increasing in size and colliding with greatly vegetated stretches, reducing dune migration speed. At this point, the small barchan/barchanoid dunes overlap larger dunes, resulting in accumulation and gradual formation of crescentic dune fields (*cf*., McKee, 1979) that may cover tens of square kilometers. Last, dune fields experience a deflationary phase where large vegetated parabolic dunes and/or large fields of parabolic dunes are formed (Carvalho *et al*., 2015).

Here the dune classification terminology compiled by Mabbutt (1977) and McKee (1979) was followed. Dune fields in the region under study also comprise large coalescing barchanoid dunes superposed by smaller barchanoid and barchan dunes (Figure 3). Crescentic dune fields usually have dimensions of hundreds of meters to kilometers. Along some places in the NE Brazilian coast these dunes merge to form a singular unit surface without a slipface, locally referred to as sand sheets (Carvalho, 2003; Carvalho *et al*., 2008; Claudino-Sales, 1993, 2002; Maia, 1998). The presence of small (few meters) and large (tens of meters) deflation surfaces are also common on these dune fields.

The two areas chosen for detailing the architecture of the cross strata are made up of wide fields of crescentic dunes, with interacting barchan and barchanoid ridges in a process detailed for other regions of the planet (*i.e*. Brothers *et al*., 2017; Day and Kocurek, 2017; Ewing and Kocurek, 2010; Ewing, McDonald, and Hayes, 2015; Fenton *et al*., 2014; Kocurek, Ewing, and Mohrig, 2010; Liu and Zimbelman, 2015; Zimbelman and Johnson, 2017). In both areas, these ridges usually migrate over a wide surface of aeolian deposits, locally called sand sheets because they do not have a slipface (Claudino-Sales, 1993, 2002; Maia, 1998). However, in some stretches these ridges migrate over a large sand body in which slipfaces are observed. In other cases, these ridges merge to form continuous barchan/barchanoid crescentic dune fields on which the ridges interact. Less common in these areas are isolated barchan and barchanoid dunes migrating over the interdune plateau. Over these larger dunes it is common for protodunes and smaller dunes to develop, which interact in a manner similar to large dunefields. Particularly between both large and small dunes, secondary wind directions develop, forming small bedforms and respective aeolian sedimentary

cross strata with dip directions outside the standard of liquid transport direction. In this study, two migrating dunes were partially isolated in Flecheiras and in the continuous crescentic dunefield in Paracuru and were studied in detail.

Compared with larger dunes of this field, these are considered to be relatively small barchanoid dunes. Dune 1 (Figure 4) is approximately 300 m wide, 230 m long, and 30 m high; and Dune 2 (Figure 4) is 300 m wide, 200 m long, and 25 m high.

METHODS
Crescentic dunes were broadly investigated along the Ceará coast, and detailed studies were concentrated along the coastal localities of Flecheiras and Paracuru, NE Brazil (Figures 1 and 4). Intensive investigations using trenches were also conducted on two dunes (Dunes 1 and 2) near Flecheiras (Figure 4), as well as on dunes and interdunes in Paracuru (Figure 4). GPR sections were conducted on the latter.

The wind rose (Figure 1) was generated using hourly wind data collected at 10 m above the surface at the Paracuru Wind Station in 2017. Wind speeds less than 5.0 m/s were not considered for wind transport. Results from Tsoar *et al*. (2009) were used for wind drift potential (DP) and Resultant Drift Potential (RDP) analyses.

Photography and Photogrammetry
Isolated dune study was done using *in situ* and remote sensing methods based on high resolution morphological characterization through 3D modelling, using a Da-Jiang Innovations (DJI) Phantom 4 unmanned aerial vehicle (UAV) with a DJI FC330 camera of 4000×3000 pixels resolution, 6.17 mm $\times$ 3.47 mm complementary metal oxide semiconductior (CMOS) sensor and 3.61 mm focal length.

The images were mainly used to mark the spatial position of small dunes, protodunes, and beveled remnants in relation to their surroundings and the larger dune surface.

UAV imaging was carried out over Dune 1 and 2 in Flecheiras and over the area of the GPR sections in Paracuru. In addition to the beveled remnants of superposed small dunes and protodunes to associate them with dip direction of internal structures, low-altitude UAV images were also used in Flecheiras and Paracuru.

Panoramic photographs obtained from a ground-level camera were also used to record the positioning and migration direction of dune ridges and beveled remnants.

Large surface characteristics, including position of the crescentic dune field slipfaces, were delineated using satellite imagery available on Google Earth (Figure 4).

In order to carry out the photogrammetric study, images from a Landsat/Copernicus satellite from 2018 were used. These images were processed and georeferenced to SIR-GAS2000/Urchin Tracking Module Zone 24S datum in a QGIS environment. To refine the georeferencing of these images, Real-time kinematic (RTK) Geodetic GPS measurements from the study area were used. In addition to these, imaging was also performed using UAV, and a digital terrain model (DTM) was developed. The resulting DTM served as an altimetric basis of aeolian morphologies and to define morphological elements associated to the characteristics of the textures and
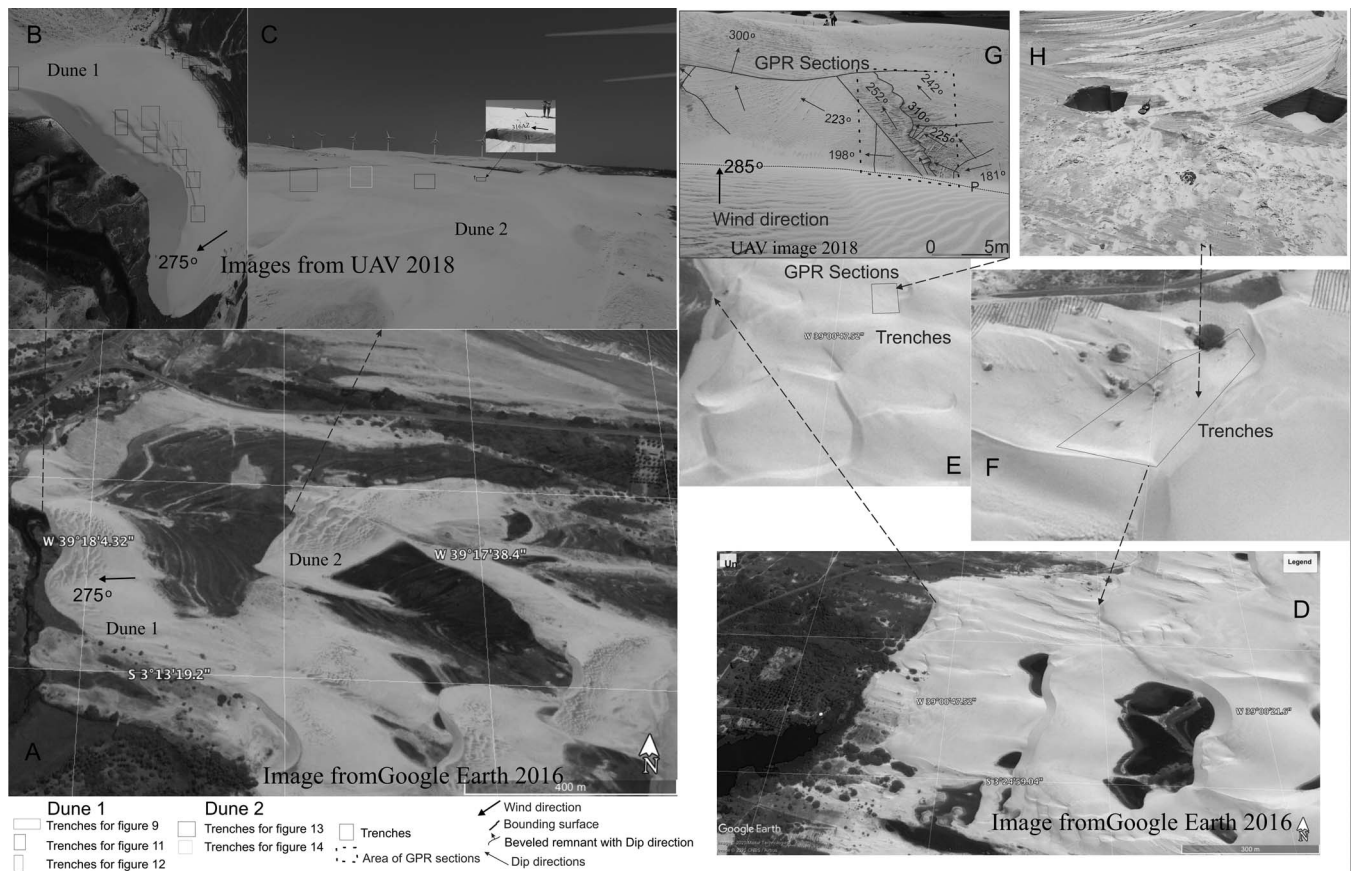
Figure 4. (A) Satellite image showing Dune 1 (300 m wide, 230 m long, and 30 m high) and Dune 2 (300 m wide, 200 m long, and 25 m high). (B) Detail of a large barchan/barchanoid surface with overlapping barchanoid crests measuring approximately 2 m in height. (C) Dune 2. The barchanoid crest distance is 10 m. B and C display the place where trenches were cut. The inset shows the location of trenches at the top of Dune 2. Dominant wind direction is marked on the image. (D) Satellite image displaying part of the Paracuru crescentic dune field. (E and F) Positioning of trenches and GPR sections. (G) Panoramic view of a deflation surface controlled by a near-surface water table. The image highlights the sequence of beveled remnants of slipfaces and a horn (P) that migrated arching up to 104° from main wind direction. (H) Surface of some trenches and the exposed remnant of cross strata in Paracuru. Directions presented in azimuth.

roughness in satellite images. The satellite images from Google Earth Pro, selected based on their representativeness and image quality, without focusing on the acquisition date, were used to illustrate figures.

Trenching, Attitude Measurement, and Grain Size Analysis

Thirty-five trenches were dug using shovels to better understand the internal structure of the dunes, especially in places where it was not possible to execute GPR sections and/or produce 3D images, and to measure cross-strata attitude. In Flecheiras (Figures 1 and 4), the work was based on several sequences of trenches: nine trenches on the base and twelve on top of Dune 1, five on top of the Dune 2 (Figure 4), where systematic strata attitude measurements of internal structures were done using a Brunton compass. Nine trenches were also dug in Paracuru (Figures 1 and 4), three of them to check dip directions displayed by the remnants of bedform migrations to check dip directions in GPR sections.

The trenches were dug in variable dimensions and shapes but were generally rectangular. In general, these dimensions were determined to cover the areas representative of the strata sizes and their dip directions, as well as the diversity of cross-strata interactions to be investigated. Often, the quantity and dimensions of the crossed strata were identified by cross-strata remnants on the surface. In general these trenches were at least 0.60 m in length, 0.40 m in width, and 0.30 m in depth.

Attitude measurements were also checked and complemented using Stereonet Mobile for iOS v. 3.0 (Allmendinger, 2017). The identification of beveled remnants of superposed dunes was useful as a strike line for locating stretches and enhancing detailed strata attitude measurements using trenches.

More than 200 strata attitude measurements were obtained from trenches cut in barchanoid dunes and along crescentic dune fields in Flecheiras and Paracuru (Figures 1 and 4). These attitude measurements were plotted on a compass rose, which was also composed of low dip angles when it was identified as real dip angles (as in the case of the base of strata). This

measurement in trenches was positioned along the dune surface, on their arms, base dune remnants, and along the interdune surface. Many trenches were also positioned on top of the large dunes. Dunes (Dune 1 and 2) in Flecheiras, selected for detailed study, are partially disconnected from the rest of the crescentic dune field.

Trenching on beveled remnants of superposed small dunes and protodunes migrating on larger ones was conducted in the case of Flecheiras (Dunes 1 and 2) and Paracuru. This was also done to analyze small- and medium-sized dune behavior as a representation for the large dune field. The easy and cheap access to internal structures and dip directions facilitates the comparison with a similar situation on a larger aeolian morphology on the satellite images. Locating the beveled remnants of barchan/barchanoid dunes is facilitated when fieldwork is conducted during the rainy season. During this time, the presence of a near-surface water table limits the level of wind deflation, as in the model proposed by Stokes (1968).

Sediment samples from surfaces of large Dunes 1 and 2, and from the trenches cut on remnants of small dunes and protodunes over Dunes 1 and 2, were collected to analyze the granulometric pattern forming these large and small dunes and protodunes. Grain size analysis was completed by dry sieving sand-sized material and pipetting the silt- and clay-sized sediments when representing a content of more than 10%. Grain size data were processed using SISGRAN software (Camargo, 2006).

Ground Penetrating Radar (GPR)

Ground penetrating radar (GPR) sections were acquired on active dune fields in Paracuru (Figure 1) to produce a 3D Cube image composition from 2D Sections to measure real dip directions and highlight cross-strata architecture. Additionally, three trenches were carried out to confirm the structures observed in the 3D GPR Cube (Figure 4).

GPR data were acquired using sections parallel to the prevailing wind direction. A 10 m × 10 m survey was covered with 10 parallel GPR lines spaced 1 m apart, recording a GPR trace every 0.05 m in order to obtain full-resolution 3D GPR surveys.

All GPR surveys were conducted using a Geophysical Survey Systems, Inc. model SIR-3000 with 200 and 400 MHz antennas. The depth of penetration is limited to less than 18 m using a 200 MHz antenna and approximately 8 m using a 400 MHz antenna, but the excellent resolution achieved has made it possible to clearly identify internal characteristics, such as cross stratifications in depths up to 8 m on a flat sandy dune surface. The sections were performed with constant spacing samplings of 40 traces per meter. When processing these data, a velocity of 0.113 m/ns determined from diffraction hyperboloid analyses with ReflexW (Sandmeier Scientific Software) was obtained for the shallow sediment cover that allowed for the parameterization of GPR depths with a mean dielectric constant of 6.94. Owing to the marked relief, topographical corrections were conducted on the GPR sections using a RTK Geodetic GPS.

RESULTS

The results obtained in this study are shown in the next paragraphs, following geographical areas:

Flecheiras

Satellite images of the crescentic dune fields in Flecheiras show interactions of barchanoid and eventually barchan crests. Secondary crests with secondary slipface dip directions to NNE and SSW (Figure 5A,B) are identified at this scale, although the wind's main direction and crestline orientations suggest an approximate migration direction to W.

In Flecheiras, near-Earth imagery shows some barchanoid crests located on the smaller dune and protodunes on top of a larger dune, such as those on Dune 1 and Dune 2 (Figure 4). These features exceed 70 m (perpendicular to the wind direction), measuring from 3 m to greater than 10 m (parallel to the wind direction) and greater than 2 m (height) in Dune 1. The southern portion of Dune 2 is marked by a straight crest with some small crests overlapping the larger one. The northern portion of Dune 2 resembles an almost disfigured barchanoid form with a flat surface with many overlying barchan/barchanoid crests measuring 2 m in height (Figure 4C).

An interaction of dune crests overlapping Dune 2 shows a dune ridge running into the back of another dune (Figure 6), which likely develops into a turbulence zone with air-flow separation (Elbelrhiti, Claudin, and Andreotti, 2005) between the windward back of the target dune (Figure 6) and the leeface of the impactor dune. Brothers *et al.* (2017) included impactor and target dunes in a class of interactions resulting in collisions between faster-migrating defects or smaller dunes, defined as impactor, and slower-migrating larger dunes defined as the target.

This interaction generates a deflation surface oriented perpendicularly to the main wind direction, hitting perpendicularly to the side of the target dune, and excavating its side until forming a slipface oriented parallel to the prevailing wind direction (Figure 6). As this slipface parallel to wind direction (Figure 6) extends to reach the back of the lee slipface of the target dune and seems to induce a flow deflection on surface winds (Hesp *et al.*, 2015), it causes this slipface to turn almost in the opposite direction to the prevailing wind. This type of interaction process and its variables are similar to the one also commonly identified on large crescent dune fields along both studied areas, expressed by large ridges perpendicular to the main wind direction, and also crests parallel to the main migration direction of the dunes (Figure 5A,B).

The internal structure pattern of the studied area consists of complex and varied cross structures, mainly plane parallel, wedge planar cross strata, and trough cross stratification. These cross-strata sets have variable thicknesses, from less than 0.05 m to more than 2 m, but are predominately at centimeter scale and mainly represent the preservation of basal portions of the cross strata.

These cross-strata dip directions show a polymodal pattern with two main directions, NNW and WSW (Figure 7). It should be noted, however, that measurements made in trench cuts were mainly concentrated in stretches of the dunes, where complex structures were identified in relation to the migration pattern of W, WNW, and WSW.

The studied aeolian deposits, positioned along with the base level of Dune 1 (Figure 4B), are composed of basal sequences of interacting small dunes. In some places, as in Figure 8, this is
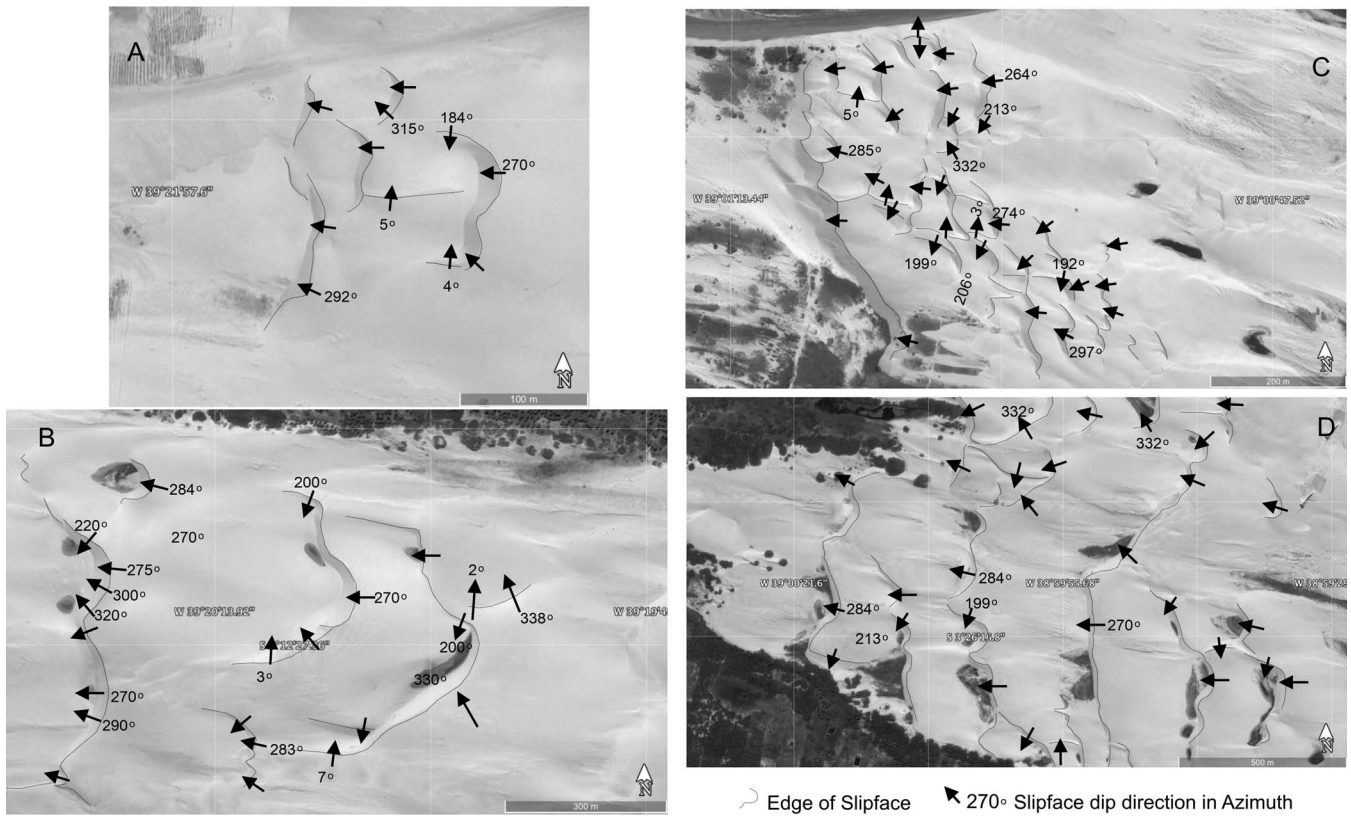
Figure 5. The orientation of the dune's slipface (indicated by arrows) on medium and large dune features from satellite imagery of Flecheiras (A and B) and Paracuru (C and D). Directions presented in azimuth.

displayed by the beveled remnants of migration marks originated by small interacting barchan/barchanoid dune crests. In Figure 8, a target dune (probably a barchanoid) was truncated by an impactor dune (a barchan).

Trench 1 (Figure 8) displays the almost horizontal set of the previous target dune on the base overlapped by the sequence of two sets of moderate and high dip angles, in the sense of McKee and Bigarella (1979). The middle set, with an apparent dip of
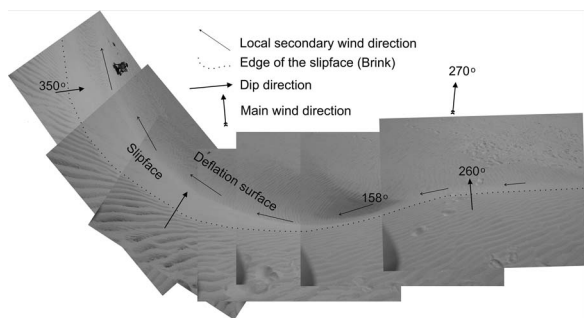

Figure 6. Development of a deflation surface cutting the side of an overlying barchan on Dune 2 and creating a slipface parallel to the wind direction. Directions presented in azimuth.
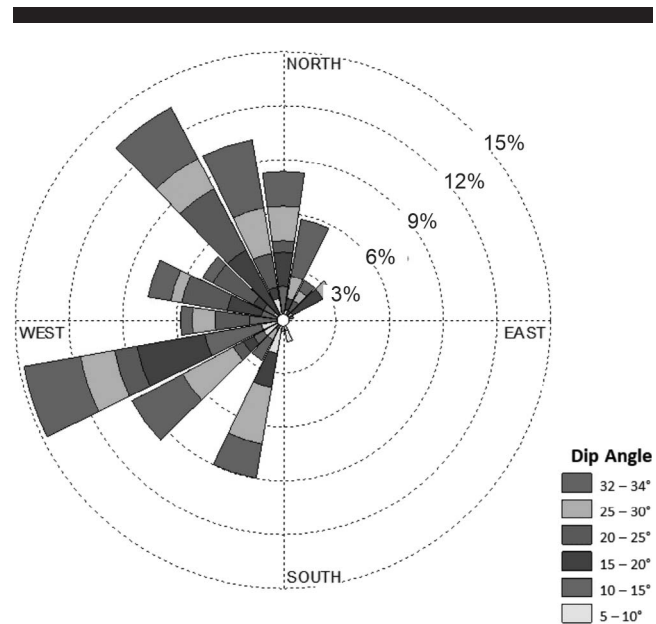

Figure 7. Cross-strata dip directions from trenches in dune deposits along Flecheiras and Paracuru. (Color for this figure is available in the online version of this paper.)
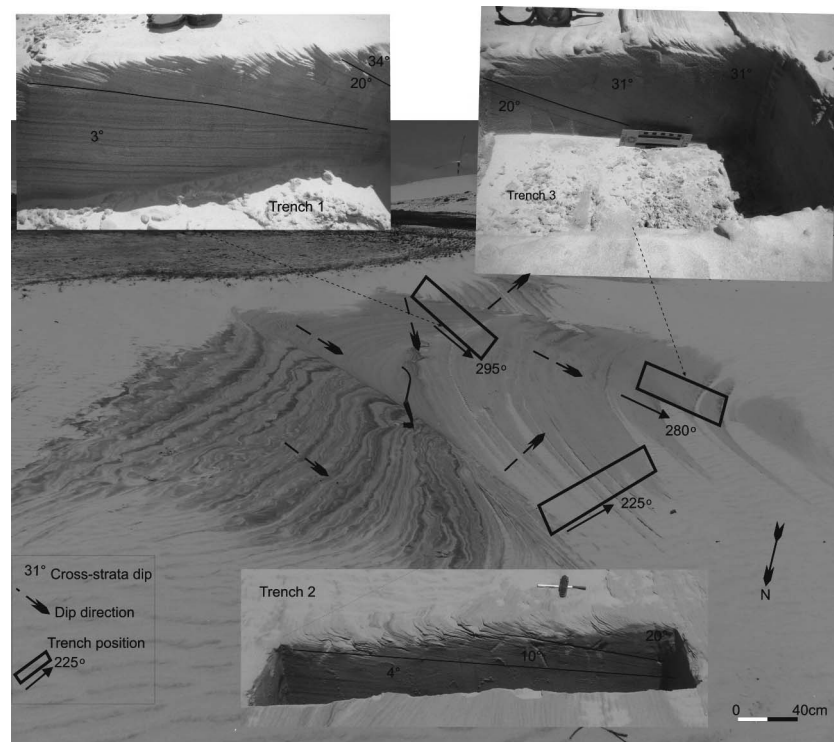
Figure 8. Beveled remnants of dune migration originated by an interacting small barchan/barchanoid dune. Base of Dune 1 in Flecheiras. Trench 1 and 2 shows the almost horizontal base strata of the target dune overlapped by the sets of high dip angles. Trench 3 shows a sequence of two foresets of moderate and high dip angles. Directions presented in azimuth.

about 20/295, records the impactor dune in relation to the basal set that hit a target set of barchanoid dunes. The top set, with 34/295, also records an impactor dune that hit both previous sequences.

Trench 2 (Figure 8) records the almost horizontal base strata from the target dune, with the trench cut almost perpendicularly to the set of the barchanoid dune migration orientation. But overlying this previous target strata dune there is a sequence of two sets displaying a moderate apparent dip angle of about 10/225 and 20/225. The first set, with a lower dip angle, records the target base set, and the one with a higher dip angle represents a small change in the dip direction of the slipface, or the last impactor strata.

Trench 3 (Figure 8) displays a sequence of two sets with moderate and high dip angles cut parallel to the barchan dune migration direction. The lower set, with a 20/280, is covered by the set of the higher dip angle of 31/280. The upper set is the new impactor dune that truncated and covered the entire previous sequence, as shown in Figure 8.

This base layer in trenches 1 and 2 (Figure 8) shows low apparent downwind dip angles (3/295 and 4/225).

The base of Dune 1 is composed of moderately sorted medium-sized quartz sand, intercalated with moderate levels of heavy minerals. The basal layer is truncated by intercalations of moderately sorted fine quartz sand, which has a lighter color compared with the base layer (Figure 8) and comprises heavy minerals. In addition, the sediments at the top of Dune 1

(Figure 4B) are composed of fine well-sorted quartz sand with heavy minerals.

On the top of Dune 1, the erosional surface of the overlaying barchan/barchanoid crests, exposing beveled remnants, and the trenches cut on it, reveals complex structures formed by sequences of interacting barchan/barchanoid crests.

Depositional sequences resulting from grain flow associated with grain fall strata (*e.g.*, Kindler *et al.*, 2011; Kocurek and Dott, 1981; McKee, 1979) are commonly observed (Figure 9A). The high dip angle at the T1B sample place is orthogonal to the other set of high dip angles on the image's right side, where grain flow is also associated with grain fall strata. In the middle (Figure 9A, sample T1), there is an almost horizontal grain flow (cut perpendicularly to the right layer dip direction), which also exhibits grain flow associated with grain fall strata.

Analyzing the interaction of small dune/protodune crests on the top of large Dune 1, there is a successive process of cutting/deflation and deposition/superposition of barchan/barchanoid dune and protodune deposits. In this process, when a more windward sinuous part of the faster-migrating barchanoid ridge bends forward, it may cover part of another barchanoid crest (Figure 10A3) and divide it into two crests resembling individual barchans (Figure 10A1,A4).

This process produces a new dune ridge further ahead in a process similar to the one presented by Kocurek, Ewing, and Mohrig (2010) and Brothers *et al.* (2017) as a defect or bedform repulsion, or even a simply faster crest covering and surpassing
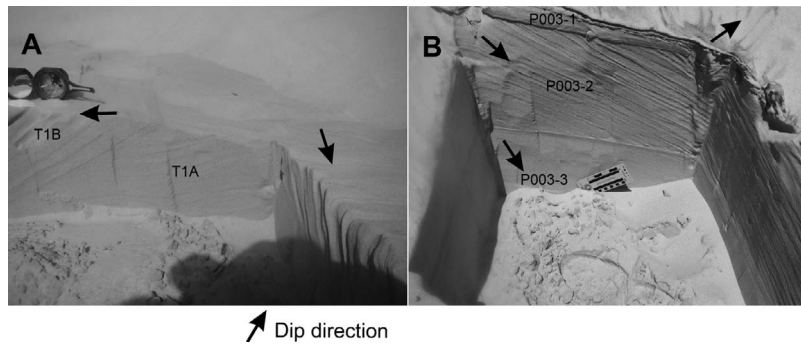
Figure 9. (A) Top of Dune 1: T1B sample place. Two sets of high dip angles, one orthogonal to the other. Both formed by grain flow associated to grain fall. (B) Top of Dune 2: High apparent cross-strata dip. Grain fall associated with grain flow strata in the middle of the image (sample P003-2). There is a smaller apparent dip angle on the base (sample P003-3) and for the top layers (sample P003-1).
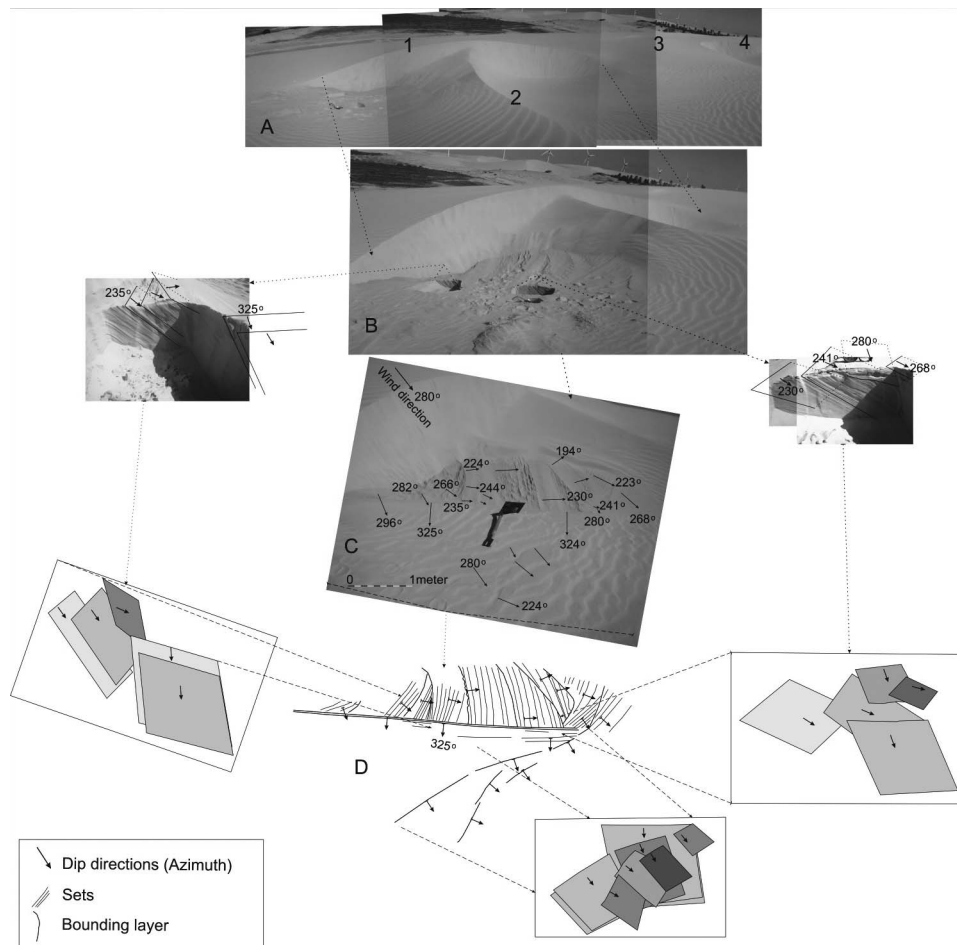

Figure 10. Beveled remnants of an overlaying barchanoid dune (Dune 1) in front of a changing barchanoid with a horn (A2) migrating perpendicularly or obtusely to the main slipface. (A1 and A4) Two crests resembling barchans on the left and on the right corner of the picture, divided by one crest (A3) that migrated over the previous barchanoid crest that previously connected the two crest A1 and A4 and formed another barchan form, not seen in this picture. (B) Detail of barchan form, the perpendicular horn, and two trenches exemplifying dip directions. (C) General dip directions. (D) Modeling of part of the cross strata based on attitude data measured in the trenches. On this site, the angle between the dip directions arc about 131° between two dip directions. Directions presented in azimuth.
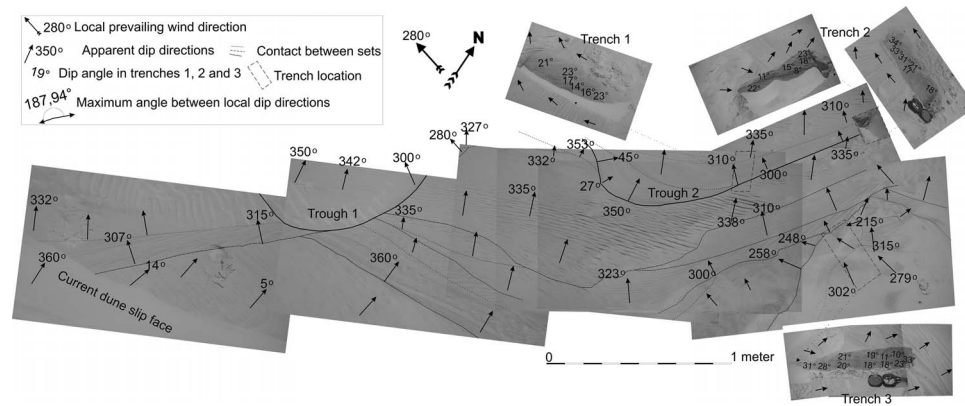
Figure 11. A panoramic view showing a deflation surface on the top of Dune 1 controlled by the near-surface water table. Beveled remnant sequences of riding barchanoid migration surfaces marking tabular sequences truncated by trough cross strata are visible (Trough 1 and 2). Dip directions are confirmed by trenches, as exemplified by Trenches 1, 2, and 3 and others not shown in this image. Directions presented in azimuth.

another forward crest. It is also common to observe small barchan crests gradually turning into barchanoids while depositing their sets of trough cross stratification. This is due to the constant variation in the migration direction of small bedform filling cuttings on the top surface of major dunes.

A migrating dune crest overlaying another dune crest ahead is also observed, resulting in a partial burial of the dune crest as shown in Figure 10A2. This process produces sets with dip directions arcing about 131°, as seen in Figure 10C. To the west in Figure 10, dip directions arcing through more than 180° were registered (Figure 11).

This process is here attributed to air-flow separation (*e.g.*, Elbelrhiti, Claudin, and Andreotti, 2005) or a flow deflection of surface winds (Hesp *et al.*, 2015) induced by a superposed bedform, thus resulting in a secondary wind direction.

This secondary wind direction can also push the crest's exposed part, and a new slipface is developed (Figure 10A2) and migrates perpendicularly or obtusely to the main dune slipface (see projected dip directions of the sets trenched in Figure 10C).

This kind of strata is also seen in Figure 11, placed west of the area of Figure 10A (see Figure 4A,B). These secondary wind directions are also widely shown on satellite images (Figure 5).

The small crest shaped like a closed half-moon, shown in Figure 10A4, seems to be responsible for the formation of the kind of trough cross stratification (Trough 1) seen in Figure 11. This trough cross strata, with an apparent barchan form, associated with the other trough cross-stratification (Trough 2), displays a migration framework of barchanoid crests.

Figure 11 also exposes a panoramic view of main dip direction sets composed of tabular sets dipping between 307° to 315° (dip directions confirmed by trenches), truncating another tabular set dipping to 360°; both sets truncated by a trough strata (Trough 1).

The center of the image (Figure 11) displays a tabular layer indicating a general migration to NNW. This layer was truncated by the cut-and-fill trough cross-stratification sequence, which exhibits dip direction arcing from 300° to 27° (Trough 2) and highlights a slight truncation dipping to 45°(NE). This slight truncation also resembles a smooth

variation in the direction of migration, or it may be a crest like the one shown in Figure 10A2. However, in the case of Figure 10A2, dip directions reach 194° (SSW) (Figure 10C). These dip directions, measured at the same dune, show the possibility of generating cross strata tending toward opposite dip directions, arcing from SSW to NNE, as also seen in Figure 5.

The top of Dune 2 (Figure 4C) is composed of well-sorted quartz thin sand intercalated with moderate levels of heavy minerals. Trenches in Dune 2 revealed that the sediments found in the base and middle layers consisted of well-sorted quartz sand, while the top layer was composed of moderately sorted quartz sand (P003-1, P003-2, and P003-3) (Figure 9B).

The cross strata in trenches on the top of Dune 2 show grain flow associated with grain fall strata in the middle layer and grain fall in the basal layer (Figure 9B).

On the top of Dune 2, crest interaction developing a deflation surface was observed, also seen in Figure 6, generating a slipface parallel to the main wind direction. This slipface also extends until it intercepts the leeward slipface of the target dune, developing a slipface dip direction of 51° (Figure 12A).

The variations in dip directions shown by the beveled remnant sequences of overlying barchan/barchanoid crests are confirmed by trenches 1 and 2 (Figure 12). A comparison of the positioning of the beveled remnant of dune cross strata with the positioning of dune slipfaces (using satellite imagery, low-altitude images, and field work (Figures 5 and 12)) confirms their compatibility with internal structures exposed in trenches. The strata show higher dip angles (True dip) since the trench is cut closely perpendicular to the beveled remnants (strike), as seen in Figures 10, 11, 12, and 13.

In Figure 13, Trench 2 (wall T2-1, set A) has higher dip angles of grain flow associated with grain fall strata, dipping to 243°, parallel in view to the real dip direction (perpendicular to remnants lines). This same set, cut perpendicularly to the dip direction in Trench 2 (wall T2-2, left of the picture), shows the limits of grain flow associated with grain fall strata (Figure 13). On the right side of wall T2-2, the other set, B, also formed by grain fall associated with grain flow cross strata, dips to about
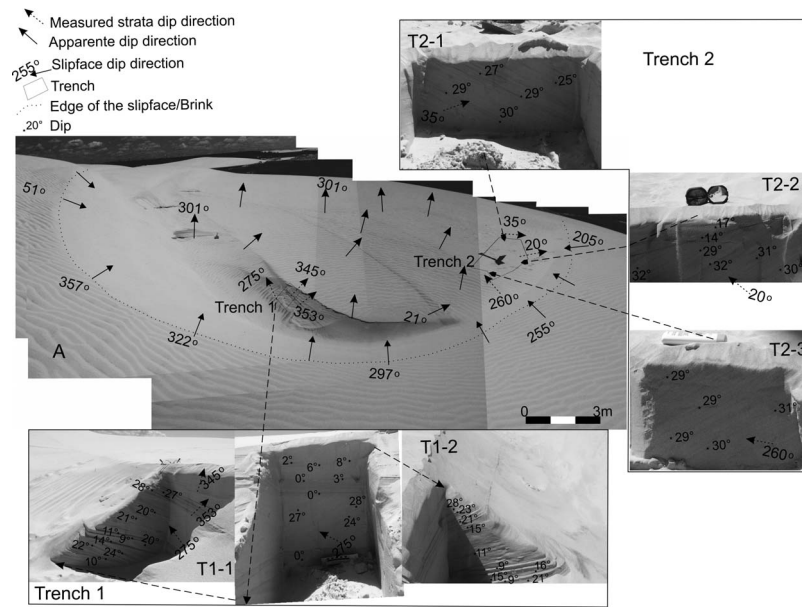
Figure 12. Details of Dune 2. (A) A panoramic view of small crest interaction on the barchanoid dune top. It also shows many truncated beveled remnant sequences of overlapping barchan/barchanoid crest migration directions and the trenches' placement. Detail of the surface and positions of Trenches 1 and 2. Directions presented in azimuth.

284° (Figure 13), and wall T2-3 shows the horizontal and subhorizontal dip of set B in a perpendicular view to dip direction. In the middle of the photo, the contact between the two sets, A and B, is highlighted. This contact also shows the transition between these two slipface directions, marked by bottom set A (dipping to 243°) being truncated by upper set B (dipping to 284°), although there seems to be a certain intersection between the sets at the top of Trench 2, wall T2-2 (Figure 13).

Figure 13 (Trench 1 and trench wall T1-3) shows a detailed trench cut almost parallel to the top layer dip direction with a high apparent dip angle and tangential contact with another layer at this base. T1-2 displays truncated sets cut perpendicularly and almost perpendicular to the dip directions, and T1-1 confirms the small and large variation on dip direction.

The contact between two perpendicular dip strata (Figure 13B and Trench 1) and the one almost perpendicular in Trench 2 shows at least one slipface migrated parallel to the prevailing wind direction associated with the other slipface that migrated perpendicularly to that, as also seen in beveled remnant sequences (Figure 13A,B).

The group of sets displayed in trenches (Figures 12 and 13) confirms suggested dip directions displayed by the remnants on its surface and also matches the position displayed by crest interactions shown in Figure 5A,B.

Paracuru

Satellite images of the crescentic dune fields in Paracuru also display interactions of barchanoid and eventual barchan crests and secondary crests. Secondary slipfaces also dip direction to NNE and SSW (Figure 5C,D), and the main wind direction and crestline orientations are to W.

In a restricted area in Paracuru (Figure 4G), several slipface sequences display azimuth dip directions arcing through 130°. However, arcs reach 180° between dip directions when extending the measurements for the total area analyzed in Paracuru (Figure 5C,D). The beveled remnant set sequences of overlaying barchanoid migration crests draw sequences of tabular and trough cross stratification with dip directions confirmed by trenches.

In Paracuru (Figure 4D,E,F,G,H), some strata sequences in trenches display a large number of truncated sets. The trench base (Figure 14A, P4 sample) is the thicker set (more than 0.8 m in thickness) of this section and is composed of well-sorted fine sized aeolian quartz sand intercalated with levels of heavy minerals. The stratum is tabular-planar with a high dip angle of about 30/260, and it is truncated by a sequence of rhythmic trough cross strata, varying in thickness from about 0.02 to 0.04 m, alternating layers of lighter and darker moderately sorted fine quartz sand, which grows from the bottom up (Figure 14A, P3), forming a set of 0.30 m in thickness and an apparent dip of about 18/351. These previous sets are truncated by another trough cross-strata set composed of light well-sorted fine sized quartz sand (Figure 14A, P2) of about 0.20 m thickness and low apparent dip angle (17/320).

This last set is also truncated by another trough cross-strata set of about 0.15 m thick fine sand composed of light mineral with a low apparent dip angle (17/277) (Figure 14A, P1). It is truncated by another set of trough cross-strata sets that follow each other showing small variations in the direction of deposition. Most of these sets are truncated by a bounded layer dipping north (Figure 14A).

Figure 14B shows the main large-scale set of tabular strata, with a 28/330 attitude, truncated by a trough cross-strata set
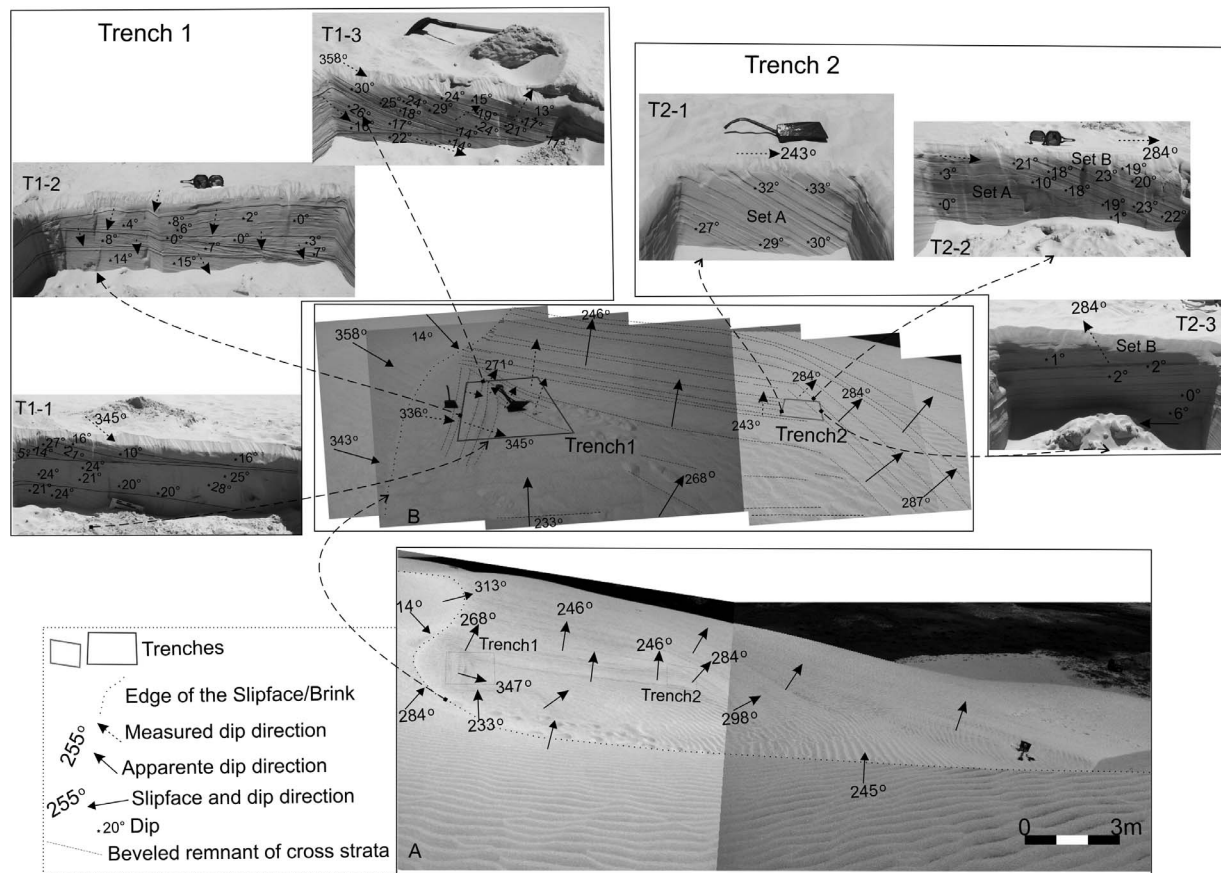
Figure 13. Details of Dune 2. (A) Panoramic view of part of the interacting dune crests; (B) Panoramic view showing many truncated beveled remnants sequences of barchanoid crest migration directions and trench placement. The top panels of (B) show details of the trench walls. The high apparent dip of grain fall associated with grain flow strata is shown in Trench 2. Directions presented in azimuth.

with 18/260, and several other trough cross strata dipping in different dip directions. This sequence of cross strata forms a set of dip directions arcing through 144° between dip directions.

Sets that are rougher on the surface are observed to be generally related to grain flow strata. As seen in Figure 14A,B, some strata sequences in trenches display a large number of truncated sets with different dip directions, mainly in an arc of up to around 60° (Figure 14A,B). Orthogonal dip directions are also easily identified, and cross strata tending to dip in opposite directions with dip azimuths arcing through more than 100° are common (Figure 14B). Panoramic surfaces locate two trenches separated 30 m from each other in Paracuru. Both images (Figure 14A,B) show sequences of tabular and trough cross strata with dip directions arcing through 174° for the sets of dip directions measured for the two trench locations.

The diversity of cross-strata dip directions is also easily identified in the GPR 3D Cube (Figure 15). These sections were performed on the area as shown in Figure 5G in Paracuru. An area of about 10×10 m^2 on an active interdune surface was covered immediately at lee side of a barchanoid dune crest. These sections, grouped in 3D, highlight a sequence of cross-strata architecture dipping to WSW, WNW, and SSW. The

strata sequence expresses the variations in migration directions of the slipfaces.

In the 3D dip direction sets, predominate cross strata in intervals between dip directions form an arc of around 60°. Orthogonal contacts are also found, and the interval between dip directions also arc through 129°.

Although most of the sets represent a cross-strata base, following McKee and Bigarella (1979), it was determined that moderate dip angles (15°–25°) are the pattern, although high dip angles (28°–29°) are common (Figure 15). The sets captured by GPR sections and represented in 3D are tabular, with the exception of set 6 (in purple), counting from top to bottom (Figure 15), which displays a trough cross strata. In this case, the attitude was also measured in a trench.

DISCUSSION

The dunes systems in the referred coastal region, effectively migrating landward, are conditioned by the relationship between the coastline's position and the effective wind direction to WSW (Carvalho *et al.*, 2015). This causes sediment to migrate from the beach toward the mainland from a specific stretch downdrift of the headlands, resulting in a sequence of characteristic dune type evolution.
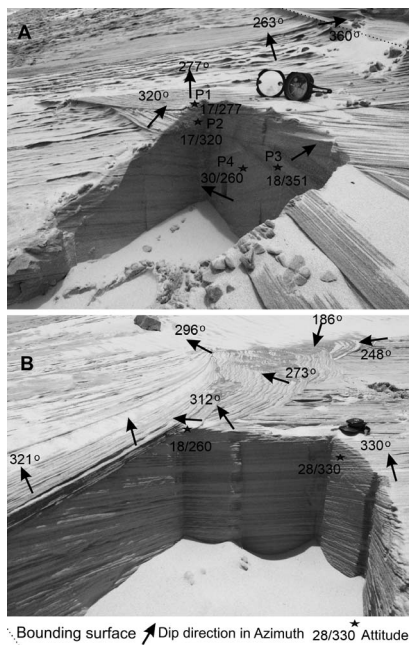
Figure 14. Panoramic surface locating two trenches separated 30 m from each other in Paracuru. A and B show sequences of tabular and trough cross strata with many dip directions. The maximum angle between dip directions in B arc through 144°, and through 174° if dip directions measured for both A and B locations is included. P1, P2, and P3 are sampling points, and directions are presented in azimuth.
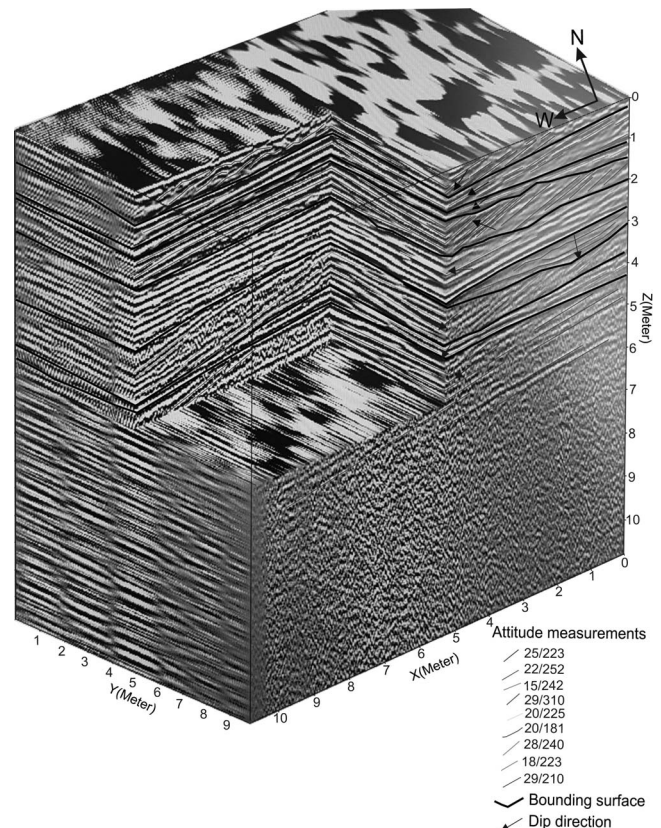

Figure 15. 3D GPR Cube composition from 2D Sections, showing nine sets of aeolian cross-strata architecture. (Color for this figure is available in the online version of this paper.)

Satellite images of the crescentic dune fields in Flecheiras and Paracuru (Figure 5) show interactions of barchanoid and, eventually, barchan crests, mainly migrating to WSW and WNW, as well as secondary crests positioned to NNE and SSW. This diversity in slipface dip direction and, consequently, strata dip direction, is also evidenced by the cross-strata azimuth measurements in trenches (Figures 10, 11, 12, 13, and 14) and 3D GPR (Figure 15).

The types and complexities of internal structures found in this crescentic dune field can be explained by ENE to ESE winds (Figure 1B). Under this assumption, one expects dunes to move arcing from WSW to WNW, with slipface dip azimuths arcing through about 60°. Along the studied coastal stretches of Paracuru and Flecheiras (Figure 1A), planar tabular cross strata with dip azimuths arcing through about 60° are dominant in these crescentic dune depositions, followed by the cross strata dipping to the azimuth arcing through 90° between dip directions. Trough type, wedge-shaped planes, and parallel and tangential contacts were frequently identified. The presence of smaller dune crests overtopping larger ones, and interacting crests, increases the range of slipface dip directions from NNE to SSW (Figure 7), which produces slipface dip azimuths arcing through 180° between dip directions. These data reveal polymodal patterns with WNW and WSW as main directions, and NNW, NNE, and SSW as secondary directions. Major directions represent the main migration direction of large slipfaces, while the secondary ones are related to smaller slipfaces, especially trough cross strata developed between

larger ridges. Allen (1962) and Harms and Fahnestock (1965) concluded that thin sets are deposited by small dunes or bedforms, and thick sets by larger dunes. In this sense, trenches in Flecheiras (Figures 10, 12, and 14) and Paracuru (Figure 14) show larger sets on the meter scale, present dip directions positioned within the range of 60° (WSW to WNW), which is in the effective wind direction. On the other hand, most thin sets, considered here as the result of a secondary slipface, usually present dip directions forming a range of 90° to 180° between dip directions. This secondary slipface and its resultant cross strata are developed by superposed bedforms inducing air-flow deflection of surface winds, resulting in a secondary wind direction. In this sense, geological records of complicated variations in aeolian cross-strata dip directions are not uncommon in the literature. Crabaugh and Kocurek (1993), studying Entrada Sandstone, identified "scalloped bounding surfaces truncating foresets to the SW, and interpreted as resulting from superimposed dunes migrating NW and SE along slope larger bedforms that migrated toward the SW". On the other hand, Havholm and Kocurek (1988), following the dynamic of a modern draa, found that second-order bounding surface orientations indicate resultant primary palaeowind directions; compound cross-strata dip directions indicate secondary flow conditions; and also considered cross-strata

0   Carvalho *et al.*

dip directions oblique or perpendicular to the second-order surface indicate longitudinal secondary flow on the lee face.

The presence of more complicated cross strata leeward of the large ridges, as presented by Crabaugh and Kocurek (1993) and Havholm and Kocurek (1988), explains the lack of expected main dip directions to the W and WNW (Figure 7) as related to the trenches' locations, concentrated between crests.

The presence of moisture rising by capillary forces to the top of the dunes acts as a limiting factor for a wind-blown deflation surface and also reveals the migration marks of superposed dune ridges on crescentic dunes. These marks are interpreted as beveled remnants (McKee, 1979) of various dune crests that result from the combination of deposits from crest interactions with different dip directions, previously dug and truncated by the leeward wind. This combination occurs, for example, when migrating slipfaces undergo changes, such as the crests of a small barchanoid overtopping another barchanoid or barchan dunes with different slipface migration directions intersecting each other.

The strata preservation, continuously attacked by secondary winds scouring unconsolidated dune sediments, is facilitated by the presence of moisture rising by capillary. This limiting control of the aeolian deflation process caused by near-surface water tables is compatible with the model proposed by Stokes (1968). The wind deflation surface, also described by Fryberger, Schenk, and Krystinik (1988), forms a downward scour limit through the cohesion of damp or wet sand near the water table. The relationship between water table or moisture variations and the formation and preservation of cross stratification sequences with different dip directions has been observed locally in the cross strata of small thickness found in trenches and GPR sections.

The influence of surface moisture on aeolian entrainment and sediment transport is well recognized in the literature (*e.g.*, Davidson-Arnott *et al.*, 2008; Nield, Wiggs, and Squirrell, 2011; Wiggs, Baird, and Atherton, 2004). Wind exceeding the threshold for transport deflates the dunes' surfaces until the water table is reached. Only when the water table or moisture of exposed surface sands dries out does additional aeolian transport take place. These surfaces are gradually covered by a new slipface migrating over them and preserving part of the crossed strata. This process repeats itself as the new dunes' crests continue to migrate. Thus, recording this migration activity is only possible after the dunes are fixed or when deposits are covered by new layers.

CONCLUSIONS

The present study along the NE coast of Brazil demonstrated that multiple spatial and temporal field-based methodologies can provide an explanation basis for variable dune crest positions, resulting in a wide range of cross-strata dip directions in a unidirectional wind system. The different slipface dip positions found within the crescentic dune using satellite and UAV imagery was confirmed by dip direction measurements in cross strata in trenches and GPR sections. This finding reveals the complicated dynamics of these dune fields and associated morphologies under unidirectional winds and highlights the possibility of recording these sedimentary structures over time. The morphology and evolution of the

crescentic dune field, in association with the multiple aeolian bedform interaction and superposition of barchanoid/barchan crests, explains the majority of structures and the wide range of strata dip directions in this unidirectional coastal wind regime.

This study also demonstrates convincing evidence that variations resulting from changing wind directions, caused by the dunes' morphology, explain much of the uncommon dip directions for unidirectional wind conditions, especially those cross strata in which dip azimuths tend to form an arc through 180°. The presence of near-surface water tables limiting the deflation level, and consequent preservation of the structures immediately covered by new deposits, suggests their importance in the formation and preservation of aeolian sequences of internal structures. The findings in this study have the potential to contribute to developing an understanding of the complex stratigraphic record that gave rise to many analogous ancient deposits worldwide.

ACKNOWLEDGMENTS

The authors thank CNPq, Science without borders (CSF), Institute of Marine Sciences, LABOMAR-UFC, and FUNCAP.

LITERATURE CITED

Allen, J.R.L., 1962. Asymmetrical ripple marks and the origin of cross-stratification. *Nature*, 194, 167–169.

Allmendinger, R.W., 2017. *Stereonet Mobile for iOS* v. 3.0. Ithaca, New York: R.W. Allmendinger, 39p.

Bagnold, R.A., 1941. *The Physics of Blown Sand and Desert Dunes*. London: Methuen and Co., 265p.

Barrineau, P. and Ellis, J.T., 2013. Sediment transport and wind flow around hummocks. *Aeolian Research*, 8, 19–27.

Bauer, B.O. and Davidson-Arnott, R.G.D., 2002. A general framework for modeling sediment supply to coastal dunes including wind angle, beach geometry, and fetch effects. *Geomorphology*, 49, 89–108.

Bauer, B.O.; Walker, I.J.; Baas, A.C.W.; Jackson, D.W.T.; Neuman, C.; Wiggs, G.F.S., and Hesp, P.A., 2013. Critical reflections on the coherent flow structures paradigm in aeolian geomorphology. *In:* Venditti, J.G.; Best, J.L.; Church, M., and Hardy, R.J. (eds.), *Coherent Flow Structures at Earth's Surface*, 1st ed. New York: Wiley, pp. 11–134.

Bigarella, J.J., 1971. Wind pattern deduced from dune morphology and internal structure. *Boletim Paranaense de Geociências*, 28/29, 73–114.

Bigarella, J.J., 1975. Lagoa dune field (State of Santa Catarina, Brazil), a model of aeolian and pluvial activity. *Bolteim Paranaense de Geociências*, 33, 133–167.

Bigarella, J.J.; Becker, R.D., and Duarte, G.M., 1969. Coastal dune structures from Paraná (Brazil). *Marine Geology*, 7, 5–55.

Bishop, S.R.; Momiji, H.; Carretero-Gonzalez, R., and Warren, A., 2002. Modelling desert dune fields based on discrete dynamics. *Discrete Dynamics in Nature and Society*, 7(1), 7–17.

Bristow, C.S.; Chroston, P.N., and Bailey, S.D., 2000. The structure and development of foredunes on a locally prograding coast: Insights from ground-penetrating radar surveys, Norfolk, UK. *Sedimentology*, 47, 923–944.

Bristow, C.S. and Pucillo, K., 2006. Quantifying rates of coastal progradation from sediment volume using GPR and OSL: The Holocene fill of Guichen Bay, south-east South Australia. *Sedimentology*, 53(4), 769–788.

Bristow, C.S.; Pugh, J., and Goodall, T., 1996. Internal structure of aeolian dunes in Abu Dhabi determined using ground-penetrating radar. *Sedimentology*, 43, 995–1003.

Brookfield, M.E., 1977. The origin of bounding surfaces in ancient aeolian sandstones. *Sedimentology*, 24, 303–332.

Brothers, S.C.; Kocurek, G.; Brothers, T.C., and Buynevich, I.V., 2017. Stratigraphic architecture resulting from dune interactions: White Sands Dune Field, New Mexico. *Sedimentology*, 64, 686–713.

Camargo, M.G. de., 2006. Sysgran: Um sistema de código aberto para análises granulométricas do sedimento. *Revista Brasileira de Geociências*, 36(2), 371–378.

Carvalho, A.M., 2003. *Dinâmica costeira entre Cumbuco e Matões-Costa NW do Estado do Ceará. Ênfase nos processos eólicos*. Salvador: Universidade Federal da Bahia, Ph.D. dissertation, 188p.

Carvalho, A.M.; Claudino-Sales, V.; Maia, L.P., and Castro, J.W.A., 2008. Eolianites of Flecheiras/Mundaú, Northwestern Coast of Ceará State, Brazil—An unique record of a coastal aeolian paleo-system. *In:* Winge, M.; Schobbenhaus, C.; Berbert-Born, M.; Queiroz, E.T.; Campos, D.A.; Souza, C.R.G., and Fernandes, A.C.S. (eds.), *Geological and Palaeontological Sites of Brazil*. Brasilia, Brazil: SIGEP, 10p. http://sigep.cprm.gov.br/sitio118/sitio118english.pdf.

Carvalho, A.M.; Ellis, J.T.; Lamothe, M., and Maia, L.P., 2015. Using wind direction and shoreline morphology to model sand dune mobilization. *Journal of Coastal Research*, 32, 1005–1015.

Castro, J.W.A.; Malta, J.; Miguel, L.L.A.J.; Cabral, C.L., and Pessamilio, A.B., 2017. Chronological reconstruction of eolianites and transversal mobile dunes of northwest coast of Ceará State, Brazil, in the last 3000 cal yrs BP. *Aeolian Research*, 28, 51–57.

Chepil, W.S., 1959. Equilibrium of soil grains at the threshold of movement by wind. *Proceedings, Soil Science Society of America*, 23, 422–428.

Claudino-Sales, V., 1993. Cenários litorâneos: natureza e ambiente na Cidade de Fortaleza, Ceará. São Paulo: University of São Paulo, Master's thesis, 357p.

Claudino Sales, V., 2002. Les littoraux de l'Etat du Ceará. Du long terme au courtterme. Paris: Université Paris Sorbonne, Ph.D. dissertation, 523p.

Clemmensen, L.B.; Bjrnsen, M.; Murray, A., and Pedersen, K., 2007. Formation of aeolian dunes on Anholt, Denmark since AD 1560: A record of deforestation and increased storminess. *Sedimentary Geology*, 199, 171–187.

Climate Variability and Predictability, Brasil (CLIVAR/BRASIL)., 1998. Um programa nacional do clima. Versão preliminar. 78p.

Cooke, R.U. and Warren, A., 1973. *Geomorphology in Deserts*. London: B. T. Batsford Ltd.

Crabaugh, M. and Kocurek, G., 1993, The dynamics and environmental context of aeolian sedimentary systems. *Geological Society Special Publication*, 72, 103–126.

Davidson-Arnott, R.G.D.; Yang, Y.; Ollerhead, J.; Hesp, P.A., and Walker, I.J., 2008. The effects of surface moisture on aeolian sediment transport threshold and mass flux on a beach. *Earth Surface Processes and Landforms*, 33(1), 55–74.

Day, M. and Kocurek, G., 2017. Aeolian dune interactions preserved in the ancient rock record. *Sedimentary Geology*, 358, 187–196.

Durán, O. and Herrmann, H.J., 2006. Vegetation against dune mobility. *Physical Review Letters*, 97, 188001.

Durán, O.; Schwammle, V., and Herrmann, H.J., 2005. Breeding and solitary wave behavior of dunes, *Physical Review E*, 72, 021308.1–021308.5.

Durán, O.; Schwammle, V.; Lind, P.G., and Herrmann, H.J., 2009. The dune size distribution and scaling relations of barchan dune fields. *Granular Matters*, 11, 7–11.

Elbelrhiti, H.; Andreotti, B., and Claudin, P., 2008. Barchan dune corridors: Field characterization and investigation of control parameters. *Journal of Geophysical Research*, 113 (F02S15).

Elbelrhiti, H.; Claudin, P., and Andreotti, B., 2005. Field evidence for surface-wave-induced instability of sand dunes. *Nature*, 437, 720–723.

Ewing, R.C. and Kocurek, G.A., 2010. Aeolian dune interactions and dune-field pattern formation: White Sands Dune Field, New Mexico. *Sedimentology*, 57, 1199–1219.

Ewing, R.C.; McDonald, G.D., and Hayes, A.G., 2015. Multi-spatial analysis of aeolian dune-field patterns. *Geomorphology*, 240, 44–53.

Fenton, L.K.; Michaels, T.I.; Chojnacki, M., and Beyer, R.A., 2014. Inverse maximum gross bedform-normal transport 2: Application to a dune field in Ganges Chasma, Mars and comparison with HiRISE repeat imagery and MRAMS. *Icarus*, 230, 47–63

Fryberger, S.G.; Schenk, C.J., and Krystinik, L.F., 1988. Stokes surfaces and the effects of near-surface groundwater-table on Aeolian deposition. *Sedimentology*, 35, 21–41.

Girardi, J.D., 2005. A GPR and Mapping Study of the Evolution of an Active Parabolic Dune System, Napeague, New York. New York: Stony Brook University, Ph.D. dissertation.

Harms, J.C. and Fahnestock, R.K., 1965. Stratification, bed forms, and flow phenomena, with an example from the Rio Grande. *In:* Middleton, G.V. (ed.), *Primary Sedimentary Structures and Their Hydrodynamic Interpretation*. SEPM Special Publication, 12, 84–115.

Havholm, K.G. and Kocurek, G., 1988, A preliminary study of the dynamics of a modern draa, Algodones, southeastern California, USA. *Sedimentology*, 35(4), 649–669.

Hersen, P.; Andersen, K.H.; Elbelrhiti, H.; Andreotti, B.; Claudin, P., and Douady, S., 2004. Corridors of barchan dunes: Stability and size selection, *Phys. Rev. E*, 69, 011304.1–011304.12.

Hesp, P.A.; Davidson-Arnott, R.; Walker, I.J., and Ollerhead, J., 2005. Flow dynamics over a foredune at Prince Edward Island, Canada. *Geomorphology*, 65, 71–84.

Hesp, P.A.; Smyth, T.A.G.; Nielsen, P.; Walker, I.J.; Bauer, B.O., and Davidson-Arnott, R., 2015. Flow deflection over a foredune. *Geomorphology*, 230, 64–74.

Horwitz, M. and Wang, P., 2005. Sedimentological characteristics and internal architecture of two overwash fans from hurricanes Ivan and Jeanne. *Gulf Coast Association of Geological Societies Transactions*, 55, 342–352.

Hsu, J.R.C; Silvester, R., and Xia, Y.M., 1989, Static equilibrium bays: New relationships. *Journal of Waterway, Port, and Coastal Ocean Engineering*, 115(3), 285–298.

Jackson, D.W.T.; Bourke, M.C., and Smyth, T.A.G., 2015. The dune effect on sand-transporting winds on Mars. *Nature Communications*, 6, 8796, 1–5.

Jimenez, J.A.; Maia, L.P.; Serra, J., and Morais, J., 1999. Aeolian dune migration along the Ceara coast, north-eastern Brazil. *Sedimentology*, 46, 689–701.

Kindler, P.; Godefroid, F.; Curran, H.A.; Dupraz, C.H.; Mylroie, J.E.; Strasses, A., and Verrecchia, E.P., 2011. Modern and quaternary carbonate environments. *Proceedings of the ESPP Bahamas Workshop 2011* (San Salvador, Bahamas), 115.

Kocurek, G.; Carr, M.; Ewing, R.; Karen G.; Havholm, K.G.; Nagar, Y.C., and Singhvi, A.K., 2007. White sands dune field, New Mexico: Age, dune dynamics and recent accumulations. *Sedimentary Geology*, 197, 313–331.

Kocurek, G. and Dott, R.H., 1981. Distinctions and use of stratification types in the interpretation of Aeolian sand. *Journal of Sedimentary Petrology*, 51, 0579–0595.

Kocurek, G.; Ewing, R.C., and Mohrig, D., 2010. How do bedform patterns arise? New views on the role of bedform interactions within a set of boundary conditions. *Earth Surface Processes and Landforms*, 35, 51–63.

Kok, J.F.; Parteli, E.J.F.; Michaels, T.I., and Karam, D.B., 2012. The physics of wind-blown sand and dust. *Reports on Progress in Physics*, 75, 106901 (72p).

Kroy, K.; Sauermann, G., and Herrmann, H.J., 2002. Minimal model for aeolian sand dunes. *Physical Review E*, 66, 031302.

Levin, N.; Tsoar, H.; Herrmann, H.J.; Maia, L.P., and Claudino-Sales, V., 2009. Modelling the formation of residual dune ridges behind barchan dunes in North-east Brazil. *Sedimentology*, 56, 1623–1641.

Li, B.; Ellis, J.T., and Sherman, D.J., 2014. Estimating the impact threshold for wind-blown sand. *In:* Green, A.N. and Cooper J.A.G. (eds.), *ICS 2014 Proceedings (Durban, South Africa). Journal of Coastal Research*, Special Issue No. 70, pp. 627–632.

Liu, Z.Y.-C. and Zimbelman, J.R., 2015. Recent near-surface wind directions inferred from mapping sand ripples on Martian dunes. *Icarus*, 261, 169–181.

Mabbutt, J.A., 1977. *Desert Landforms*. Cambridge, Massachusetts: MIT Press, 340pp.

Maia, L.P., 1998. Procesos costeiros y balance sedimentario a lo largo de Fortaleza (NE-Brasil): Implicações para una gestión adecuada

de la zona litoral. Barcelona: Universitat de Barcelona, Ph.D. dissertation, 269p.

Martin, R.L.; Kok, J.F.; Hugenholtz, C.H.; Barchyn, T.E.; Chanecki, M., and Ellis, J.T., 2018. High-frequency measurements of aeolian saltation flux: Field-based methodology and applications. *Aeolian Research*, 30, 97–114.

McKee, E.D., 1966. Structures of dunes at White Sands National Monument, New Mexico (and a comparison with structures of dunes from other selected areas). *Sedimentology*, 7, 1–69.

McKee, E.D., 1979. A Study of Global Sand Seas. U.S. Geological Survey Professional Paper no. 1052. Reston, Virginia: U.S. Geological Survey.

McKee, E.D. and Bigarella, J.J., 1979. Sedimentary structures in dunes, Chapter E. *In:* Edwin D. McKee, A Study of Global Sand Seas. U.S. Geological Survey Professional Paper no. 1052. Reston, Virginia: U.S. Geological Survey.

Mountney, N.P., 2012. A stratigraphic model to account for complexity in aeolian dune and intervene successions. *Sedimentology*, 59, 964–989.

Narteau, C.; Zhang, D.; Rozier, O., and Claudin, P., 2009. Setting the length and time scales of a cellular automaton dune model from the analysis of superimposed bed forms. *Journal of Geophysical Research*, 114, 1–18.

Nield, J.; Wiggs, G.F.S., and Squirrell, R.S., 2011. Aeolian sand strip mobility and protodune development on a drying beach: Examining surface moisture and surface roughness patterns measured by terrestrial laser scanning. *Earth Surface Processes and Landforms*, 36(4), 513–522.

Pelletier, J.D.; Sherman, D.J.; Ellis, J.T.; Farrell, E.J.; Jackson, N.J.; Li, B.; Nordstrom, K.F.; Maia, L.P., and Omidyeganeh, M., 2015. Dynamics of sediment storage and release on aeolian dune slip faces: A field study in Jericoacoara, Brazil. *Journal of Geophysical Research: Earth Surface*, 120(9), 1911–1934.

Rubin, D.M., 1987. *Cross-bedding, Bedforms and Paleocurrents*. Tulsa, Oklahoma: Society of Economic Paleontologists and Mineralogists Concepts in Geology, 187p.

Sauermann, G.; Andrade Jr., J.S.; Maia, L.P.; Costa, U.M.S.; Araújo, A.D., and Herrmann, H.J., 2003. Wind velocity and sand transport on a barchan dune. *Geomorphology*, 54(3–4), 245–255.

Schwämmle, V. and Herrmann, H.J., 2004. Modelling transverse dunes. *Earth Surface Processes and Landforms*, 29, 769–784.

Sherman, D.J.; Li, B.; Ellis, J.T.; Farrell, E.J.; Maia, L.P., and Granja, H., 2013. Recalibrating aeolian sand transport models. *Earth Surface Processes and Landforms*, 38, 169–178.

Sherman, D.J.; Li, B.; Ellis, J.T., and Swann, C., 2018. Intermittent aeolian saltation: A protocol for quantification. *Geographical Review*, 108(2), 296–314.

Silvester, R., 1960. Stabilization of Sedimentary Coastline. *Nature*, 188 (4749), 467–469.

Silvester, R., 1970. Growth of crenulate shaped bays to equilibrium. *Journal of the Waterways and Harbor Division, American Society of Civil Engineers*, 76, 275–287.

Silvester, R. and Ho, S.K., 1972. Use of crenulate-shaped bays to stabilize coasts. *Proceedings of the 13th Coast Engineering Conference, American Society of Civil Engineers* (Reston, Virginia), pp. 1347–1365.

Sorby, H.C., 1859. On the structures produced by the currents present during the deposition of stratified rocks. *Geologist*, 2, 137–147.

Stokes, W.L., 1968. Multiple parallel-truncation bedding planes: a feature of wind-deposited sandstone formations. *Journal of Sedimentary Petrology*, 38(2), 510–515.

Tsoar, H.; Levin, N.; Porat, N.; Maia, L.P.; Herrmann, H.J.; Tatumi, S.H., and Claudino-Sales, V., 2009. The effect of climate change on the mobility and stability of coastal sand dunes in Ceará State (NE Brazil). *Quaternary Research*, 71, 217–226.

Wiggs, G.F.S.; Baird, A.J., and Atherton, R.J., 2004. The dynamic effects of moisture on the entrainment and transport of sand by wind. *Geomorphology*, 59, 13–30.

Wright, L.D. and Short, A.D., 1983. Morphodynamics of beaches and surf zones in Australia. *In*: Komar, P.D. (ed.), *Handbook of Coastal Processes and Erosion*. Boca Raton, Florida: CRC Press, pp. 35–64.

Yasso, W.E., 1965. Plan geometry of headland-bay beaches. *Journal of Geology*, 73(5), 702–719.

Zimbelman, J.R. and Johnson, M.B., 2017. Surface slope effects for ripple orientation on sand dunes in López crater, Terra Tyrrhena region of Mars. *Aeolian Research*, 26, 57–62.